Photochemical & Photobiological Sciences

PAPER

Cite this: *Photochem. Photobiol. Sci.*, 2018, **17**, 51

New insight into an efficient visible light-driven photocatalytic organic transformation over CdS/TiO_2 photocatalysts†

Zengzeng Hu, Huanhuan Quan, Zhen Chen, Yu Shao and Danzhen Li *

Received 5th July 2017,
Accepted 10th November 2017

DOI: 10.1039/c7pp00256d

rsc.li/pps

Selective transformation of organics by visible-light-driven photocatalysis has been considered as a green and efficient strategy for the synthesis of fine chemicals. Herein, we fabricated mesoporous structured TiO_2 with CdS nanoparticles successfully by a photodeposition method. The photocatalytic selective oxidation of benzyl alcohols and reduction of 4-nitroaniline were demonstrated over the as-prepared samples under visible-light irradiation. The CdS-decorated TiO_2 with the photodeposition time of 90 min exhibited highest activity, which was higher than that of the commercial CdS, bare TiO_2, CdS/P25, and CdS/SiO_2. Further experimental results indicated that the higher performance was attributed to the moderate deposition of CdS forming a closely connected heterojunction with TiO_2, which promoted the separation of photogenerated electrons and holes. Based on the results of active species detection, possible mechanisms for photocatalytic selective oxidation of benzyl alcohol and reduction of 4-nitroaniline were proposed. Our study may provide guidance for selective transformation of organics *via* construction of heterojunction photocatalysts.

Introduction

In the past several years, heterogeneous photocatalysis as an efficient and environmental technique has attracted interest in the remediation of environment and artificial photosynthesis of organic compounds.[1–5] Specifically, photocatalytic organic transformation can fundamentally eliminate the problems of high energy consumption and serious pollution existing in chemical production. To date, numerous photocatalysts, such as various oxide and sulfide semiconductors and polymers, have been developed for photocatalytic organic synthesis.[6–9] Among them, TiO_2 is the most used photocatalyst because it is non-toxic and has good stability and high photocatalytic activity. However, most of the applications of TiO_2 were limited to the UV-light range (only occupying 3–4% of sunlight) because of the large bandgap of TiO_2.[10] When TiO_2 is endowed with visible-light response, its photocatalytic efficiency dramatically improves.[11–13]

For this purpose, combining TiO_2 with various narrow-band-gap semiconductors has been considered as an efficient way.[13–16] Among various semiconductors, CdS was an excellent visible-light-driven photocatalyst and widely used to couple with TiO_2 to form CdS/TiO_2 nanocomposites. Many previous studies have reported that the CdS/TiO_2 nanocomposites can exhibit improved photocatalytic efficiency under not only UV light but also visible light irradiation.[13,17–19] However, the synthesized CdS/TiO_2 nanocomposite often suffered from the lack of an effective heterojunction structure; this led to the rapid recombination of photogenerated carriers and prevented further improvement of the photocatalytic performance of CdS/TiO_2.[20–24] Therefore, synthesis of a CdS/TiO_2 photocatalyst with an effective heterojunction structure still remains a challenge.

Herein, we have prepared mesoporous structured TiO_2 nanoparticles successfully, and CdS has been tiled on TiO_2 *via* a facile photodeposition method. Photodeposition could utilize the photoinduced electrons from the mesoporous structure TiO_2 to the synthesized CdS; this assured a high specific surface area and inherent combination of uniform distribution of CdS on TiO_2. High-resolution transmission electron microscopy showed that the CdS/TiO_2 heterostructure was formed. The photocatalytic activity of CdS/TiO_2 was evaluated by the photocatalytic selective oxidation of alcohols to aldehydes and selective reduction of nitroaromatic compounds to amino organics. A comparison of the photocatalytic performance of the CdS/TiO_2 heterostructure with those of reported materials under visible light is shown in Table S1,† and it is observed that CdS/TiO_2-90 possesses the best conversion for

State Key Laboratory of Photocatalysis on Energy and Environment, Research Institute of Photocatalysis, Fuzhou University, Fuzhou 350002, P. R. China. E-mail: dzli@fzu.edu.cn; Fax: (+86)591-83779256

†Electronic supplementary information (ESI) available. See DOI: 10.1039/c7pp00256d

aerobic oxidation of benzyl alcohol to benzaldehyde when benzotrifluoride (BTF) is used as a solvent. In addition, the possible reaction mechanisms for the two photocatalytic reactions have been proposed based on the results of radical detection and scavenger experiments. It is hoped that this study can provide us guidance for selective transformation of organics *via* construction of heterojunction photocatalysts.

Experimental

Materials

Titanium isopropoxide(TIP), cadmium chloride ($CdCl_2{\cdot}2.5H_2O$), sulfur (S_8), commercial CdS (Co-CdS), commercial TiO_2 (P25), and ammonium formate (HCO_2NH_4) were purchased from Sinopharm Chemical Reagent Co. Ltd. Benzotrifluoride (BTF) was obtained from Alfa Aesar China Co. Ltd. Isopropyl alcohol (IPA) was of analytical grade and purchased from the Shanghai Chemical Co. All chemicals and solvents were of analytical grade and used as received without further purification.

Preparation of TiO_2

TiO_2 was synthesized through a hydrothermal method post calcination. First, 12 ml of H_2O and 42 ml of IPA were mixed together to form a solution. Then, 5 ml of TIP was added dropwise to the abovementioned solution under continuous stirring. After several minutes of stirring, the mixture was transferred into a Teflon-lined stainless steel autoclave. The autoclave was sealed and heated in an oven at 120 °C for 12 h. After being cooled down naturally, the obtained precipitate was centrifuged, washed with deionized water and anhydrous ethanol several times, and then dried at 60 °C for 12 h. Finally, the precipitate was calcined at 200 °C for 4 h in a muffle furnace.

Photodeposition of CdS on TiO_2

The suspension of TiO_2 (100 mg) in absolute ethanol (52 ml) that included $CdCl_2{\cdot}H_2O$ (60 mg) and S_8 (9 mg) was bubbled with nitrogen for 30 min in the dark. Then, the suspension was irradiated with a 500 W Xe arc lamp under incident light at $\lambda \geq 320$ nm for 30, 60, 90, and 120 min. The precipitate was centrifuged, washed with deionized water and absolute ethanol several times, and then dried at 60 °C. The synthesized samples were labeled CdS/TiO_2-30, CdS/TiO_2-60, CdS/TiO_2-90, and CdS/TiO_2-120.

Photocatalyst characterization

X-ray diffraction (XRD) patterns of the samples were obtained using a Bruker D8 Advance X-ray diffractometer operated at 40 kV and 40 mA with Cu Kα radiation. The morphology and microstructure of the obtained samples were observed by transmission electron microscopy (TEM) and high-resolution transmission electron microscopy (HRTEM, JEOL JEM-2010 EX). The Edinburgh FL/FS900 fluorescence spectrometer was used to investigate the photoluminescence (PL) spectra of samples. UV-vis diffuse reflectance spectra of the samples were obtained by a UV-vis spectrometer (Varian Cary 500). Electron spin resonance (ESR) spectra were obtained using a Bruker model A300 spectrometer with a 500 W Xe-arc lamp equipped with a cut-off filter (420 nm $\leq \lambda \leq$ 800 nm) as a light source. The photoelectrochemical measurement was conducted using a CHI-660D electrochemical workstation (CHI Instruments, Co., Shanghai). The measurement was carried out in a conventional three-electrode electrochemical cell with a platinum wire counter electrode, Ag/AgCl electrode as a reference electrode, and a working electrode. The working electrode was prepared on a fluorine-doped tin oxide (FTO) glass. Moreover, 0.1 M of Na_2SO_4 solution was used as an electrolyte.

Photocatalytic activity test

To explore the performance of the photocatalyst, a series of experiments was carried out. At first, the photocatalytic selective oxidation of different benzylic alcohols was performed as follows: 0.1 mmol of alcohol and 8 mg of photocatalyst were added to 1.5 ml of oxygen-saturated BTF. Then, the abovementioned mixture was transferred into a 10 ml Pyrex glass bottle filled with oxygen under a pressure of 0.1 MPa and stirred for 30 min to make the catalyst distribute evenly in the solution. The suspension was irradiated with a 500 W Xe-arc lamp (Institute of Electric Light Source, Beijing) with the wavelength of 420 nm $\leq \lambda \leq$ 800 nm. After the reaction, the mixture was centrifuged at 12 000 rpm for 10 min to completely remove the catalyst particles. The remaining solution was analyzed using an Agilent gas chromatograph (GC-7890). The conversion of alcohol and selectivity for aldehyde were defined as follows:

$$\text{Conversion } (\%) = (C_0 - C_{\text{alcohol}})/C_0 \times 100 \quad (1)$$

$$\text{Selectivity } (\%) = C_{\text{aldehyde}}/(C_0 - C_{\text{alcohol}}) \times 100 \quad (2)$$

where C_0 is the initial concentration of benzyl alcohol, $C_{\text{benzyl alcohol}}$ and C_{aldehyde} are the concentrations of the substrate benzyl alcohol and the corresponding aldehyde at a certain time after the photocatalytic reaction, respectively.

Next, a range of experiments for photocatalytic hydrogenation of 4-nitroaniline (4-NA) was performed. Prior to the catalytic test, 20 mg of the obtained sample was suspended in 80 ml of a 4-NA aqueous solution (10 ppm) in a Pyrex reactor (100 ml). After adding 20 mg of ammonium formate, the suspension was stirred in the dark for 30 min and bubbled with N_2 to ensure establishment of an adsorption–desorption equilibrium between the sample and 4-NA. As the reaction proceeded, 2 ml of the suspension was obtained at certain intervals and then centrifuged. The concentrations of 4-NA and *p*-phenylenediamine (PPD) during the reaction were analyzed by measuring the absorbance at 380 and 238 nm, respectively, using a Cary 50 UV-vis spectrophotometer (Varian Co.). The entire photocatalytic process was carried out under N_2 bubbling at a flow rate of 60 ml min^{-1}. The conversion of 4-NA and selectivity for PPD were defined as follows:

$$\text{Conversion } (\%) = (C_0 - C_{\text{NA}})/C_0 \times 100 \quad (3)$$

$$\text{Selectivity } (\%) = C_{PPD}/(C_0 - C_{NA}) \times 100 \quad (4)$$

where C_0 is the initial concentration of 4-NA and C_{NA} and C_{PPD} are the concentrations of 4-NA and PPD, respectively, at a certain time after the photocatalytic reaction. Furthermore, C_{PPD} was determined by a linear relationship (A = 0.069C, R^2 = 0.9991) between the absorbance (A) and the concentration (C) at 238 nm for PPD.

Results and discussion

XRD spectra and absorption spectra

Fig. 1 shows the XRD patterns of the as-prepared TiO_2 and CdS/TiO_2 at different photodeposition times. The pattern of TiO_2 could be indexed to a single anatase crystalline phase of TiO_2 (PDF#21-1272). The characteristic peaks at 25.21, 37.88, 48.02, 54.07, 55.05, 62.65, 68.82, 70.49, and 75.22° corresponded to the (101), (004), (200), (105), (211), (213), (116), (220), and (215) crystal planes, respectively. After photodeposition for 30 min, additional peaks could be observed at 28.15 and 43.88°, which were assigned to the (101) and (110) crystal planes of CdS, respectively, and were attributed to hexagonal CdS (PDF# 41-1049). Moreover, it was found that the diffraction peaks intensity of CdS increased with the increasing photodeposition time; this indicated an increase in the amount of CdS as compared to that of TiO_2.

The optical properties of the as-prepared samples were determined, and the results are shown in Fig. 2a. The absorption of TiO_2 was at the onset of about 380 nm. After the photodeposition of CdS, the absorption of CdS/TiO_2 in the visible-light region can be improved by increasing the photodeposition time; this is in accordance with the progressively intense yellow color of the samples. Fig. 2b shows the bandgap energy (E_g) of the as-prepared samples derived from the adsorption spectra using the equation as follows:

$$F(R)^* E = A(E - E_g)^{n/2} \quad (5)$$

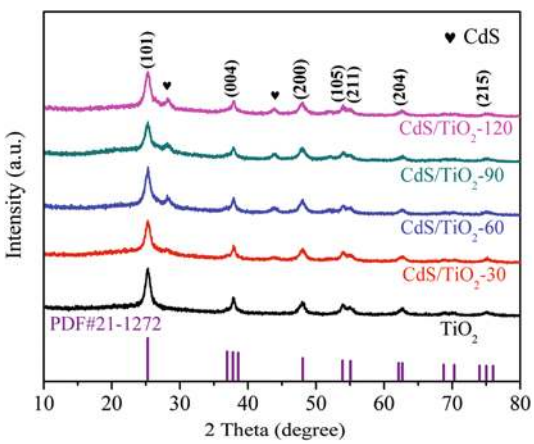

Fig. 1 XRD patterns of TiO_2 and CdS/TiO_2 at different photodeposition times.

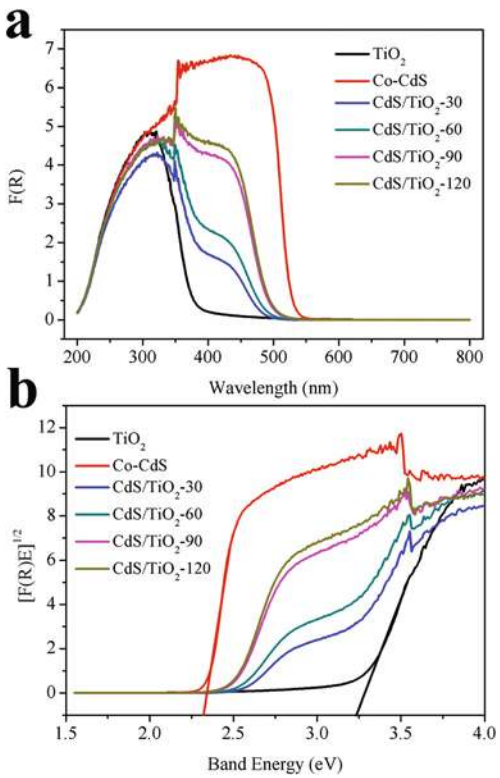

Fig. 2 (a) UV-vis diffuse reflectance spectra and (b) optical bandgap energy E_g of Co-CdS, TiO_2, and CdS/TiO_2.

where $F(R)$ is the diffuse absorption coefficient; E is the photon energy; A is the proportionality constant; n is an integer (n = 1, 2, 4, and 6), and E_g is the bandgap.[25] As observed, the bandgap of TiO_2 was estimated to be 3.21 eV and that of CdS/TiO_2 decreased with the increasing photodeposition time.

XPS spectra

Fig. 3 shows the XPS spectra of the typical sample CdS/TiO_2-90, as well as that of TiO_2 for comparison. As shown in Fig. 3a, all peaks in the wide-scan XPS spectrum of TiO_2 were ascribed to Ti, O, and C elements. The presence of C is due to the carbon film that commonly exists for XPS. After photodeposition of CdS for 90 min, an additional peak attributed to the Cd element could be observed in the XPS spectrum of CdS/TiO_2-90. The existence of S element could be verified by the high-resolution XPS spectrum of S 2p, as shown in Fig. 3b. Furthermore, the characteristic binding energies of S 2p (162.15 eV) and Cd 3d (405.08 eV for Cd $3d_{5/2}$ and 411.80 eV for Cd $3d_{3/2}$) indicated the bivalent reduction state for S and bivalent oxidation state for Cd,[17,26] which verified the formation of CdS. As shown in Fig. 3c, the Ti 2p XPS spectrum of the sample CdS/TiO_2-90 at the binding energies of 458.50 eV for Ti $2p_{3/2}$ and 464.35 eV for Ti $2p_{1/2}$ indicated a Ti^{4+} oxidation state.[27] The O 1s XPS spectrum of the sample CdS/TiO_2-90 was divided into two peaks: the peak at 529.85 eV could be attributed to the lattice oxygen and that at 531.45 eV was assigned to

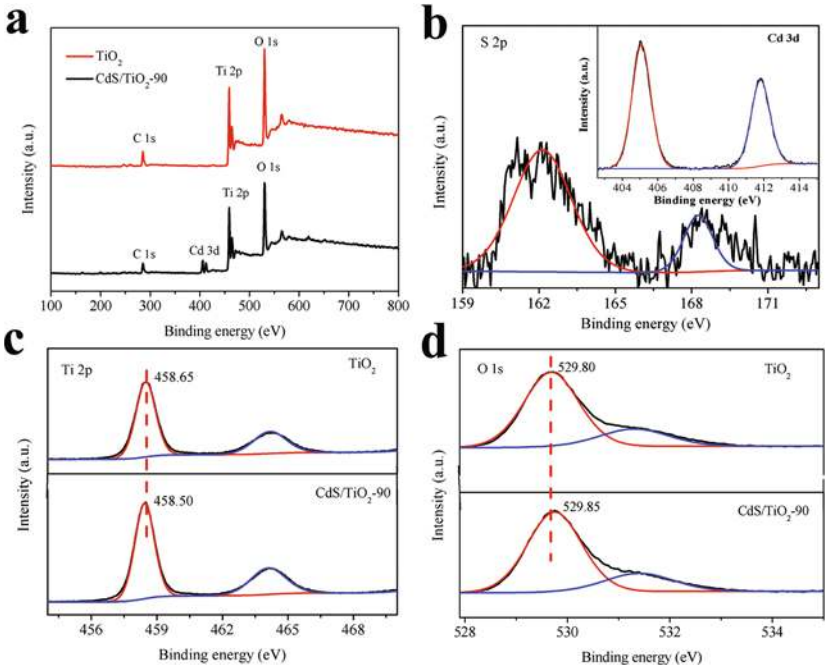

Fig. 3 (a) The wide-scan XPS spectra of CdS/TiO_2-90 and TiO_2, (b) XPS spectra of S 2p and Cd 3d (inset), the narrow-scan Ti 2p (c) and O 1s (d) XPS spectra of the sample CdS/TiO_2-90 and TiO_2.

oxygen in surface hydroxyl groups.[28] Moreover, it was noted that the peak of Ti 2p for the sample CdS/TiO_2-90 shifted towards a lower binding energy and that of O 1s shifted slightly towards a higher binding energy when compared with that for the sample TiO_2. This phenomenon could be ascribed to the formation of a heterojunction between CdS and TiO_2, which accelerated the electron transfer from CdS to TiO_2.

Nitrogen adsorption and TEM images

Fig. 4 shows the N_2 adsorption–desorption isotherms of the typical sample CdS/TiO_2-90. The sharp decline in the desorption curve indicated that CdS/TiO_2-90 exhibited a type IV adsorption–desorption isotherm. The pore size distribution in the inset manifested the narrow range of 3.0–11.0 nm with an average pore size of 5.7–6.0 nm for CdS/TiO_2-90. This result indicated that the as-prepared CdS/TiO_2 was mesoporous. Furthermore, the surface areas of TiO_2 and CdS/TiO_2 were compared, as shown in Table S2.† As observed, the surface area of TiO_2 was 201 m^2 g^{-1}. The photodeposition of CdS decreased the surface area of TiO_2 and that of CdS/TiO_2 decreased with the increasing photodeposition time. However, the as-prepared CdS/TiO_2 still exhibited a higher surface area than Co-CdS.

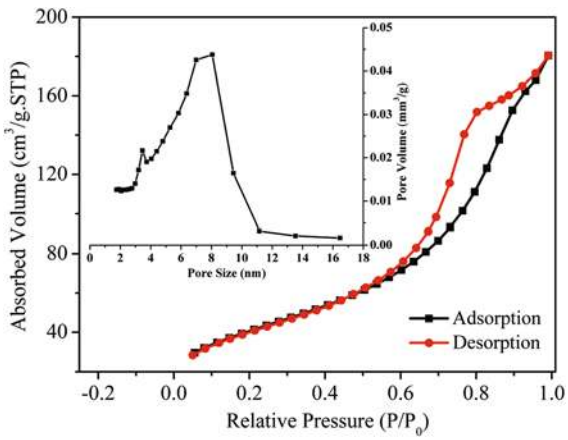

Fig. 4 N_2 adsorption–desorption isotherms and BJH pore size distribution (inset) for the sample CdS/TiO_2-90.

The morphology of the as-prepared samples was investigated by HRTEM. As shown in Fig. 5a, the TEM image of pure TiO_2 indicated a nanocrystalline morphology with an average diameter of 5 nm. The lattice interplanar spacing of d = 0.352 nm matched the (101) plane of anatase TiO_2. In addition, pores with a diameter of 3 nm could be observed; this was in agreement with the BET analysis results and further suggested a mesoporous structure in TiO_2. After photodeposition of CdS for 90 min, the TEM image of CdS/TiO_2-90 was obtained, as shown in Fig. 5b. The lattice interplanar spacing of d = 0.336 nm matched the (002) plane of CdS, which verified the existence of CdS. Furthermore, some distinct junctions between CdS and TiO_2 could be observed, which indicated the formation of the heterojunction. The heterojunction of the sample CdS/TiO_2-90 could be beneficial for improving the separation of photogenerated carriers and therefore promotes the photocatalytic performance; this has been discussed hereinafter.

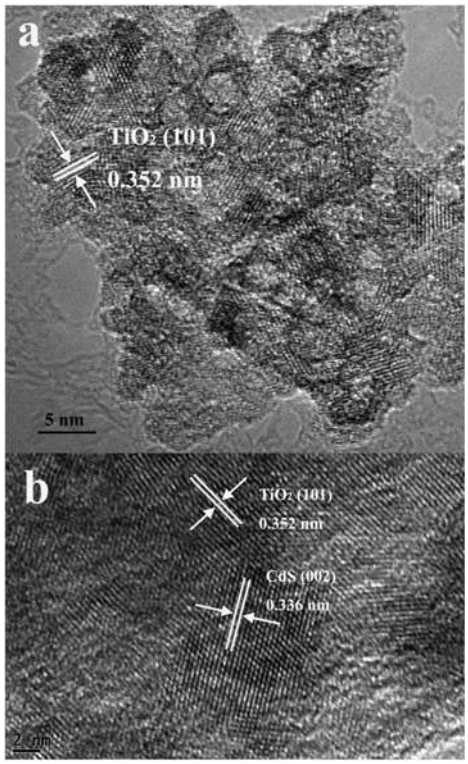

Fig. 5 HRTEM images of (a) TiO_2 and (b) CdS/TiO_2-90.

Photocatalytic performance

In this study, selective oxidation of benzyl alcohol and selective reduction of 4-NA were used as probe reactions for the as-prepared samples. At first, photocatalytic activities of the as-prepared samples for the selective oxidation of benzyl alcohol were evaluated under visible light irradiation. As shown in the Fig. 6a, TiO_2 showed a conversion of 3.52% for the selective oxidation of benzyl alcohol to benzaldehyde. After photodeposition of CdS, the photocatalytic activity could be further improved. Among them, CdS/TiO_2-90 exhibited the highest conversion of 45.03% and the selectivity of 97.03% after 4 h reaction under visible light irradiation. Moreover, it can be clearly found that photodeposition time plays a vital role in the photocatalytic activities of the as-prepared samples. Originally, prolonging the photodeposition time from 0 min to 90 min can improve the photocatalytic activity. The improved activity could be attributed to the formation of a heterojunction and increased visible-light absorption over CdS/TiO_2. On the other hand, when the photodeposition time exceeds 90 min, excess CdS would load on the surface of TiO_2; this may hinder the contact between the heterojunction and benzyl alcohol. Thus, the photocatalytic activity of CdS/TiO_2-120 decreased. Furthermore, to verify the higher activity of CdS/TiO_2-90, the selective oxidation of benzyl alcohol over Co-CdS and CdS photodeposited on P25 (CdS/P25) and SiO_2 (CdS/SiO_2) was demonstrated under the same conditions for comparison. As shown in Fig. 6b, CdS/SiO_2 showed negligible activity. The photocatalytic activity of CdS/TiO_2-90 was about 6 and 2 times higher than that of Co-CdS and CdS/P25, respectively. Moreover, the selective oxidation of different substituted benzyl alcohols over CdS/TiO_2-90 sample was investigated in this study. As shown in Table S3,† various substituted benzyl alcohols can be efficiently converted into the corresponding benzaldehydes. These results further indicated that CdS/TiO_2-90 was efficient for the selective oxidation of benzyl alcohol to benzaldehyde.

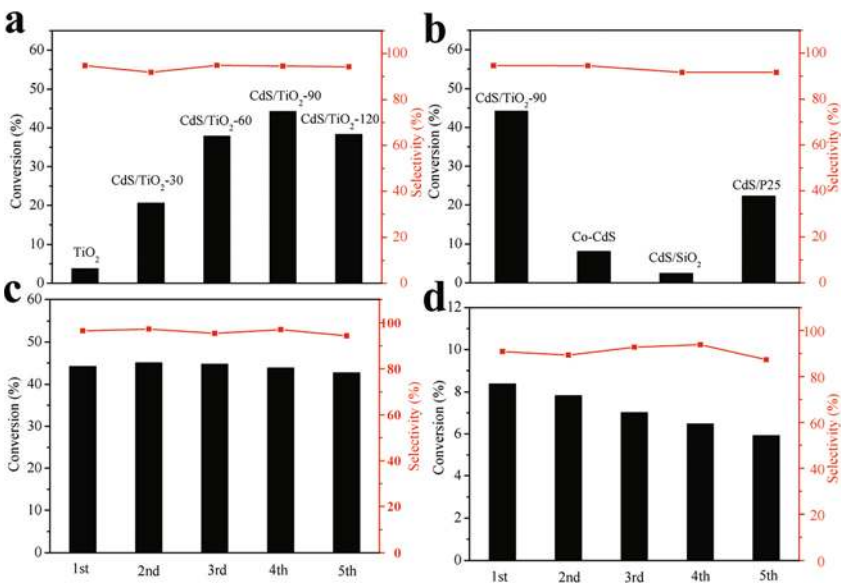

Fig. 6 (a) Photocatalytic selective oxidation of benzyl alcohol over CdS/TiO_2 with different photodeposition times; (b) photocatalytic selective oxidation of benzyl alcohol over different photocatalysts; recycling testing of the photocatalytic activity of CdS/TiO_2-90 (c) and Co-CdS (d) towards the selective oxidation of benzyl alcohol to benzaldehyde under visible light irradiation ($\lambda \geq 420$ nm) for 4 h.

It is generally known that the photocorrosion of CdS (CdS + $h^+ \rightarrow Cd^{2+} + S$) leads to a decline in the photocatalytic activity. To examine the stability of the as-prepared CdS/TiO_2, recycling experiment was conducted over the CdS/TiO_2-90 and commercial CdS. As shown in Fig. 6c, the photocatalytic activity of CdS/TiO_2-90 resulted in a high conversion of 45% and selectivity of 97% even after five cycles, whereas that of commercial CdS (Fig. 6d) decreased by 25%. This can be attributed to higher dispersity of CdS than that of Co-CdS as well as the fact that photogenerated holes tend to get involved in the reactions; thus, the photocorrosion of CdS can be relieved. This result indicated that CdS/TiO_2-90 was an efficient and stable visible-light-driven photocatalyst for the selective oxidation of benzyl alcohol to benzaldehyde.

As CdS showed excellent activity for the photocatalytic hydrogenation of 4-NA to PPD,[8] the activities of the as-prepared CdS/TiO_2 for this reaction were also evaluated under visible light irradiation. As shown in Fig. 7a, there was a rapid decrease in the absorption of 4-NA at 380 nm along with a simultaneous appearance of new peaks at 238 and 305 nm whose absorbance increased as the reaction continued.[8] This result indicated that CdS/TiO_2-90 exhibited photocatalytic activity towards 4-NA reduction. For comparison, the activities of CdS/TiO_2 with different photodeposition times, together with that of the pure TiO_2, commercial CdS, CdS/P25, and CdS/SiO_2, were investigated under similar conditions. As shown in Table 1, the conversion of 4-NA and selectivity of PPD over CdS/TiO_2-90 were higher than that of other samples. Furthermore, higher activity stability of CdS/TiO_2-90 could be observed when compared with that of the commercial CdS (Fig. 7b). On the basis of the abovementioned results, it can be concluded that CdS/TiO_2-90 can also serve as an efficient and stable photocatalyst for the selective reduction of 4-NA to PPD.

Table 1 Photoreduction performances of 4-NA over different samples

Sample	Hole scavenger	Atmosphere	Conversion (%)	Selectivity (%)
CdS/TiO_2-30	HCO_2NH_4	N_2	87.9	88.6
CdS/TiO_2-60	HCO_2NH_4	N_2	88.5	89.1
CdS/TiO_2-90	HCO_2NH_4	N_2	98.6	95.3
CdS/TiO_2-120	HCO_2NH_4	N_2	79	83.3
TiO_2	HCO_2NH_4	N_2	3.8	—
Co-CdS	HCO_2NH_4	N_2	85.7	83.3
CdS/SiO_2	HCO_2NH_4	N_2	32.9	60.9
CdS/P25	HCO_2NH_4	N_2	79.1	85.4

Enhancement of interface charge separation efficiency

A photoelectrochemical measurement was performed to further trace the enhancement mechanism for the photocatalytic activity of samples. The obtained photocurrent-time (I–t) profiles without any bias potential are shown in Fig. 8a. It could be observed that CdS/TiO_2-90 exhibited remarkably strong photocurrent intensity. Then, it was followed by CdS/TiO_2-60, CdS/TiO_2-30, and CdS/TiO_2-120, which was in good agreement with their photocatalytic activities. The higher photocurrent of CdS/TiO_2-90 could be attributed to moderate

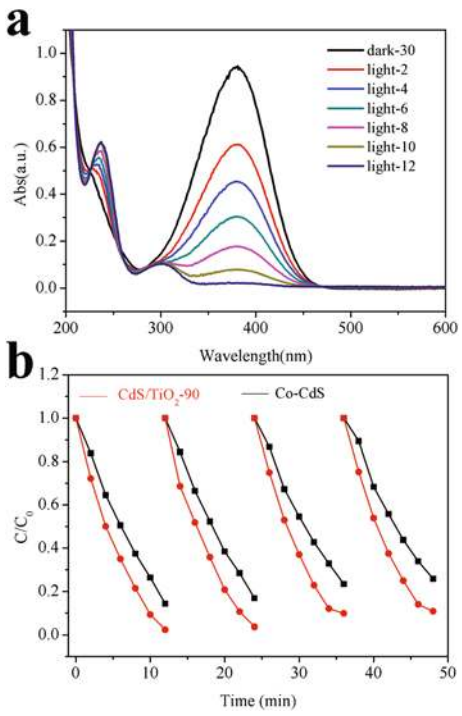

Fig. 7 (a) UV-vis spectral changes of a 4-NA aqueous solution in the sample CdS/TiO_2-90 suspension as a function of irradiation time. (b) Recycling photocatalytic reduction of 4-NA over CdS/TiO_2-90 and Co-CdS.

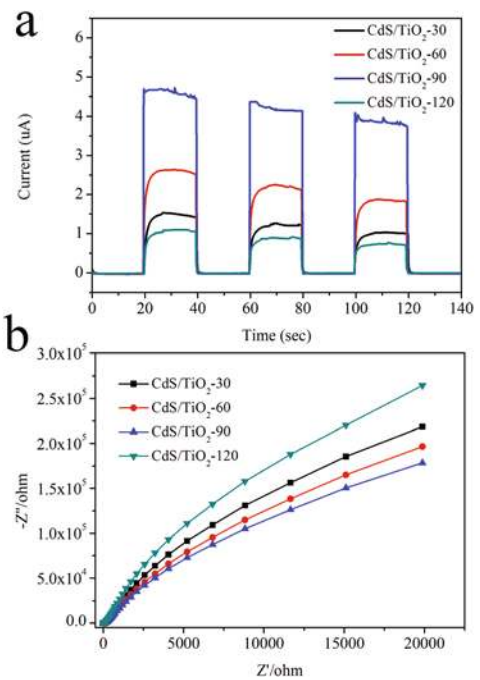

Fig. 8 (a) Photocurrent spectra without any bias potential for different samples under visible-light irradiation, (b) EIS Nyquist plots without any bias potential of the as-prepared samples.

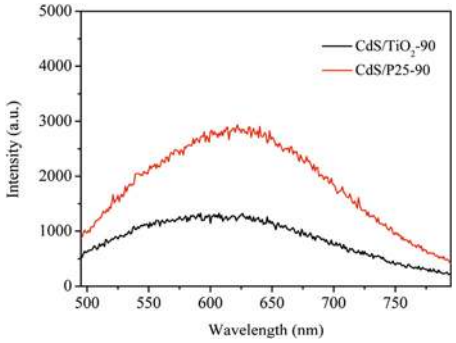

Fig. 9 Photoluminescence (PL) spectra of the sample CdS/TiO_2-90 and CdS/P25.

CdS on TiO_2 forming a closely connected heterojunction, which improved the transfer efficiency of photo-induced electrons to the conductor substrate. Electrochemical impedance spectroscopy (EIS), as shown in Fig. 8b, was also used to evaluate the separation efficiency of photogenerated charges over the catalyst. The radius of the arc on the EIS Nyquist plot represented the charge transfer step occurring on the surface of the electrode. It was clearly seen that CdS/TiO_2-90 had the minimum arc radius, which indicated good separation efficiency of photogenerated electron–hole pairs. To further investigate this, the PL emission spectra of CdS/TiO_2-90 and CdS/P25 were obtained with the excitation light of λ = 400 nm. As shown in Fig. 9, the emission peak around 590 nm could be attributed to luminescence during the recombination of electron–hole pairs of CdS. Moreover, the PL intensity of CdS/TiO_2-90 was weaker than that of CdS/P25; this further suggested the efficient separation efficiency of photogenerated electronic–hole pairs over CdS/TiO_2-90. These results confirmed the good activity of CdS/TiO_2-90 for the photocatalytic selective oxidation of alcohol and selective reduction of 4-NA.

Possible photocatalytic mechanism

To elucidate the mechanism of photocatalytic conversion of benzyl alcohol over CdS/TiO_2-90, a series of controlled experiments have been performed. As shown in Fig. 10a, when benzoquinone (BQ), a scavenger for superoxide radicals ($^{\bullet}O_2^-$), was added to the reaction system, the conversion of benzyl alcohol was obviously decreased. The addition of methanol as a scavenger for holes decreased the photocatalytic activity to a lesser extent. Negligible effect could be observed when tertiary-butanol (TBA) was added as a scavenger for hydroxyl radicals ($^{\bullet}OH$). Moreover, it was found that the conversion of benzyl alcohol was significantly inhibited when the reaction was carried out under a N_2 atmosphere. The presence of N_2 could aggravate the recombination of photo-induced carriers; this decreased the formation of holes and $^{\bullet}O_2^-$. These results indicate that the photocatalytic selective oxidation of benzyl alcohol over CdS/TiO_2-90 was driven by photogenerated holes and $^{\bullet}O_2^-$. Furthermore, the existence of $^{\bullet}O_2^-$ was confirmed by the DMPO spin-trapping ESR technique, as shown in Fig. 10b.

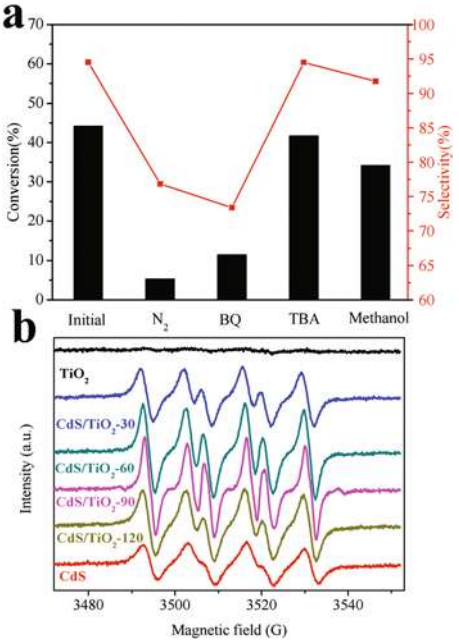

Fig. 10 (a) Photocatalytic selective oxidation benzyl over CdS/TiO_2-90 under different conditions and visible-light irradiation for 4 h; (b) DMPO spin-trapping ESR spectra for $^{\bullet}O_2^-$ under visible-light irradiation.

The characteristic sextet peaks of DMPO-$^{\bullet}O^{2-}$ adduct were more obvious over CdS/TiO_2-90 than over other samples; this further verified the good photocatalytic activity of the proposed catalyst.

Moreover, the mechanism for photocatalytic hydrogenation of 4-NA over CdS/TiO_2-90 was investigated under visible-light irradiation. As shown in Fig. 11, the characteristic sextet peaks attributed to the DMPO-$^{\bullet}CO_2^-$ adduct were observed. The formation of $^{\bullet}CO_2^-$ radicals can be attributed to the reaction between the photoexcited holes of CdS and HCO_2NH_4 ($E(HCO_2^-/^{\bullet}CO_2^-)$ = 1.07 V *vs.* NHE).[29] The $^{\bullet}CO_2^-$ radicals have strong reductive powers ($E(^{\bullet}CO_2^-/CO_2)$ = −1.9 V *vs.* NHE) and have been considered to be an active species for hydrogenation of 4-NA.[30] In addition, the photo-induced electrons of CdS transferred to the conduction band of TiO_2, which were possible active species for hydrogenating 4-NA to PPD (E(4-NA/PPD)

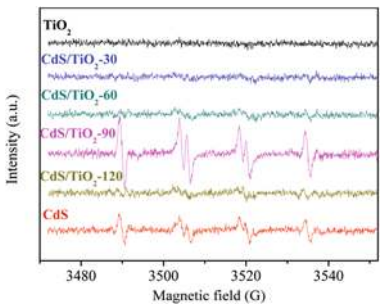

Fig. 11 DMPO spin-trapping ESR spectra for $^{\bullet}CO_2^-$ under visible-light irradiation.

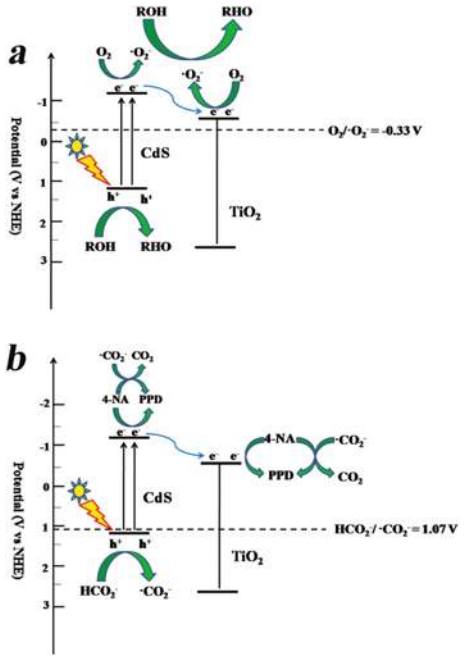

Fig. 12 Proposed mechanism for (a) photocatalytic selective oxidation of alcohols and (b) photocatalytic reduction of 4-NA over the CdS/TiO_2 nanocomposite.

= −0.68 V *vs.* NHE).[29] Furthermore, control experiment results, as shown in Fig. S2,† indicated that HCO_2NH_4 as a hole scavenger and nitrogen as a shielding gas played a very important role during the hydrogenation of 4-NA over CdS/TiO_2-90.

On the basis of the abovementioned results, the proposed mechanism for photocatalytic oxidation of alcohols and reduction of 4-NA over CdS/TiO_2 is illustrated in Fig. 12. Under visible-light irradiation, CdS was excited to generate electron–hole pairs. The photo-induced electrons can transfer to the conduction band of TiO_2 owing to its suitable band edge position, and the photo-induced holes remained in the valence band of CdS. For the photocatalytic oxidation reaction, the photo-induced electrons were captured by O_2 molecules to form $^{\bullet}O^{2-}$ radicals. Both photo-induced holes and $^{\bullet}O^{2-}$ radicals have oxidation ability for selective oxidation of alcohols. As for the photocatalytic hydrogenation reaction, the photo-induced holes can react with HCO_2NH_4 to form $^{\bullet}CO_2^-$. Both the photo-induced electrons and $^{\bullet}CO_2^-$ radicals have strong reductive ability for photocatalytic hydrogenation of 4-NA to PPD.

Conclusions

In summary, CdS/TiO_2 photocatalysts were successfully prepared by the photodeposition method. The obtained samples showed higher photocatalytic activities for the photocatalytic selective oxidation of alcohols to aldehydes and selective reduction of 4-NA to PPD under visible-light irradiation ($\lambda \geq$ 420 nm). The sample CdS/TiO_2-90 exhibited highest catalytic performance because of a closer interface and larger surface, which could improve the separation of photogenerated carriers. The improved interface charge separation efficiency could also be observed in photoelectrochemical measurement and photoluminescence spectra. Based on the abovementioned results, it can be concluded that CdS/TiO_2 has a promising prospect for selective transformation of organics.

Conflicts of interest

There are no conflicts of interest to declare.

Acknowledgements

This work was financially supported by the NNSF of China (21173047 and 21373049).

Notes and references

1 Y. G. Zhou, Y. F. Zhang, M. H. Lin, J. L. Long, Z. Z. Zhang, H. X. Lin, J. C. S. Wu and X. X. Wang, Monolayered Bi2WO6 nanosheets mimickingheterojunction interface with open surfaces for photocatalysis, *Nat. Commun.*, 2015, **6**, 8340.

2 C. J. Huang, C. Chen, M. W. Zhang, L. H. Lin, X. X. Ye, S. Lin, M. Antonietti and X. C. Wang, Carbon-doped BN nanosheets for metal-free photoredox catalysis, *Nat. Commun.*, 2015, **6**, 7698.

3 X. F. Li, X. Z. Zhen, S. G. Meng, J. J. Xian, Y. Shao, X. Z. Fu and D. Z. Li, Structuring β-Ga_2O_3 photonic crystal photocatalyst for efficient degradation of organic pollutants, *Environ. Sci. Technol.*, 2013, **47**, 9911–9917.

4 Y. Shao, C. C. Cao, S. L. Chen, M. He, J. L. Fang, J. Chen, X. F. Li and D. Z. Li, Investigation of nitrogen doped and carbon species decorated $TiO_2$with enhanced visible light photocatalytic activity by using chitosan, *Appl. Catal., B*, 2015, **179**, 344–351.

5 S. J. Liang, L. R. Wen, S. Lin, J. H. Bi, P. Feng, X. Z. Fu and L. Wu, Monolayer HNb_3O_8 for selective photocatalytic oxidation of benzylic alcohols with visible light response, *Angew. Chem., Int. Ed.*, 2014, **53**, 2951–2955.

6 C. Gao, Q. Q. Meng, K. Zhao, H. Yin, D. W. Wang, J. Guo, S. L. Zhao, L. Chang, M. He, Q. X. Li, H. J. Zhao, X. J. Huang, Y. Gao and Z. Y. Tang, Co_3O_4 hexagonal platelets with controllable facets enabling highly efficient visible-light photocatalytic reduction of CO_2, *Adv. Mater.*, 2016, **30**, 6485–6490.

7 J. G. Yu, J. X. Low, W. Xiao, P. Zhou and M. Jaroniec, Enhanced photocatalytic CO_2^- reduction activity of anatase TiO_2 by coexposed {001} and {101} facets, *J. Am. Chem. Soc.*, 2014, **136**, 8839–8842.

8 W. M. Wu, G. D. Liu, Q. H. Xie, S. J. Liang, H. R. Zheng, R. S. Yuan, W. Y. Su and L. Wu, A simple and highly efficient route for the preparation of p-phenylenediamine

by reducing 4-nitroaniline over commercial CdS visible light-driven photocatalyst in water, *Green Chem.*, 2012, **14**, 1705–1709.

9 J. Liu, J. H. Huang, H. Zhou and M. Antonietti, Uniform graphitic carbon nitride nanorod for efficient photocatalytic hydrogen evolution and sustained photoenzymaticcatalysis, *ACS Appl. Mater. Interfaces*, 2014, **6**, 8434–8440.

10 H. W. Park, H. I. Kim, G. H. Moon and W. Y. Choi, Photoinduced charge transfer processes in solar photocatalysis based on modified TiO_2, *Energy Environ. Sci.*, 2016, **9**, 411–433.

11 X. F. Yang, J. L. Qin, Y. Jiang, K. M. Chen, X. H. Yan, D. Zhang, R. Li and H. Tang, Fabrication of P25/Ag_3PO_4/graphene oxide heterostructures for enhanced solar photocatalytic degradation of organic pollutants and bacteria, *Appl. Catal., B*, 2015, **166**, 231–240.

12 R. Marotta, I. D. Somma, D. Spasiano, R. Andreozzi and V. Caprio, Selective oxidation of benzyl alcohol to benzaldehyde in water by TiO_2/Cu(II)/UV solar system, *Chem. Eng. J.*, 2011, **172**, 243–249.

13 Y. Bessekhouad, D. Robert and J. V. Weber, Bi_2S_3/TiO_2 and CdS/TiO_2 heterojunctions as an available configuration for photocatalytic degradation of organic pollutant, *J. Photochem. Photobiol., A*, 2004, **163**, 569–580.

14 Z. B. Jiao, T. Chen, J. Y. Xiong, T. Wang, G. X. Lu, J. H. Ye and Y. P. Bi, Visible-light-driven photoelectrochemical and photocatalytic performances of Cr-doped $SrTiO_3/TiO_2$ heterostructured nanotube arrays, *Sci. Rep.*, 2013, **3**, 2720.

15 C. Cheng, A. Amini, C. Zhu, Z. Xu, H. Song and N. Wang, Enhanced photocatalytic performance ofTiO_2-ZnO hybrid nanostructures, *Sci. Rep.*, 2014, **4**, 4181.

16 S. Q. Liu, M. Q. Yang and Y. J. Xu, Surface charge promotes the synthesis of large, flat structured graphene–(CdS nanowire)–TiO_2nanocomposites as versatile visible light photocatalysts, *J. Mater. Chem. A*, 2014, **2**, 430–440.

17 L. Wu, J. C. Yu and X. Z. Fu, Characterization and photocatalytic mechanism of nanosized CdS coupled TiO_2 nanocrystals under visible light irradiation, *J. Mater. Chem. A*, 2006, **244**, 25–32.

18 J. Fang, L. Xu, Z. Y. Zhang, Y. P. Yuan, S. W. Cao, Z. Wang, L. S. Yin, Y. S. Liao and C. Xue, Au@TiO_2–CdS ternary nanostructures for efficient visible-light-driven hydrogen generation, *ACS Appl. Mater. Interfaces*, 2013, **5**, 8088–8092.

19 Z. C. Lian, P. P. Xu, W. C. Wang, D. Q. Zhang, S. N. Xiao, X. Li and G. S. Li, C60-decorated CdS/TiO_2 mesoporous architectures with enhanced photostability and photocatalytic activity for H_2evolution, *ACS Appl. Mater. Interfaces*, 2015, **7**, 4533–4540.

20 Q. Yu, J. Xu, W. Z. Wang and C. L. Lu, Facile preparation and improved photocatalytic H-2-production of Pt-decorated CdS/TiO_2 nanorods, *Mater. Res. Bull.*, 2014, **51**, 40–43.

21 N. Zhang, Y. H. Zhang, X. Y. Pan, M. Q. Yang and Y. J. Xu, Constructing ternary CdS-graphene-TiO_2 hybrids on the hlatland of graphene oxide with enhanced visible-light photoactivity for selective transformation, *J. Phys. Chem. C*, 2012, **116**, 18023–18031.

22 S. J. Yu, J. C. Hu and J. J. Li, Self-assembly of TiO_2/CdS mesoporous microspheres with enhanced photocatalytic activity *via* hydrothermal method, *Int. J. Photoenergy*, 2014, **2014**, 854217.

23 X. R. Li, J. G. Wang, Y. Men and Z. F. Bian, TiO_2 mesocrystal with exposed (001) facets and CdS quantum dots as an active visible photocatalyst for selective oxidation reactions, *Appl. Catal., B*, 2016, **187**, 115–121.

24 S. Q. Liu, N. Zhang, Z. R. Tang and Y. J. Xu, Synthesis of one-dimensional CdS@TiO_2 core-shell nanocomposites photocatalyst for selective redox: the dual role of TiO_2 shell, *ACS Appl. Mater. Interfaces*, 2012, **4**, 6378–6385.

25 L. H. Yu, X. Y. Zhang, G. W. Li, Y. T. Cao, Y. Shao and D. Z. Li, Highly efficient $Bi_2O_2CO_3$/BiOCl photocatalyst based on heterojunction with enhanced dye-sensitization under visible light, *Appl. Catal., B*, 2016, **187**, 301–309.

26 N. Qin, W. M. Wu, L. J. Shen, X. Chen, Z. H. Li and L. Wu, One-dimensional CdS/TiO_2nanofiber composites as efficient visible-light-driven photocatalysts for selective organic transformation: synthesis, characterization, and performance, *Langmuir*, 2015, **32**, 1203–1209.

27 C. Y. Su, C. L. Shao and Y. C. Liu, Electrospun nanofibers of TiO_2/CdS heteroarchitectures with enhanced photocatalytic activity by visible light, *J. Colloid Interface Sci.*, 2011, **359**, 220–227.

28 M. Y. Zhang, C. L. Shao, Z. C. Guo, Z. Y. Zhang, J. B. Mu, T. P. Cao and Y. C. Liu, Hierarchical nanostructures of copper(II) phthalocyanine on electrospun TiO_2 nanofibers: controllable solvothermal-fabricationand enhanced visible photocatalytic properties, *ACS Appl. Mater. Interfaces*, 2011, **3**, 369–377.

29 W. M. Wu, R. Lin, L. J. Shen, R. W. Liang, R. S. Yuan and L. Wu, Mechanistic insight into the photocatalytichydrogenation of 4-nitroaniline over band-gap-tunable CdS photocatalysts, *Phys. Chem. Chem. Phys.*, 2013, **15**, 19422–19426.

30 X. F. Li, C. Q. Wang, B. Li, Y. Shao and D. Z. Li, Efficient light harvesting over a CdS/In_2O_3 photonic crystal photocatalyst for hydrogenation of 4-nitroaniline to p-phenylenediamine, *Phys. Chem. Chem. Phys.*, 2016, **18**, 27848–27857.